Study of the Frequency Modulations on the Optical and Structural Characteristics of Electrodeposited Ni-Doped PbTe Thin Films

Muomeliri, Chukwudi B*.; Ekpunobi, Azubuike J.; Okoli, Donald N

Department of Physics and Industrial Physics, Nnamdi Azikiwe University Awka, Anambra State, Nigeria

***Corresponding Author**

DOI: https://doi.org/10.51584/IJRIAS.2026.110200019

Received: 10 February 2026; Accepted: 18 February 2026; Published: 27 February 2026

ABSTRACT

This report presents the successful fabrication and characterization of nickel-doped lead telluride (Ni:PbTe) chalcogenide thin films for potential device applications. The films were synthesized using a three-electrode electrodeposition method on fluorine-doped tin oxide (FTO) glass substrates, with lead trinitrate (V), tellurium (IV) oxide, and nickel chloride hexahydrate serving as precursors. Deposition time was varied to optimize film properties. Characterization using UV-Vis spectrometry and X-ray diffraction (XRD) revealed that absorbance increased with deposition time across the visible (VIS) and near-infrared (NIR) regions. The refractive index ranged from 1.5–1.62 at 1-minute deposition, increasing to 2.5–3.25 at 4 minutes, indicating suitability for optoelectronic devices like optical fibers and waveguides. Transmittance decreased with longer deposition times but remained higher in the NIR region. The optical bandgap ranged from 1.3–1.7 eV across different deposition times ideal for photovoltaic and LED applications. Film thickness also increased with deposition time, suggesting that optical properties can be tuned accordingly.XRD analysis confirmed the crystalline nature of the films, with crystallinity improving at longer deposition durations. Structural parameters such as crystallite size, dislocation density, and microstrain supported this trend, reinforcing the films' potential for advanced optoelectronic applications.

Keywords: lead telluride (PbTe), Nickel, photodetector, Infrared detector, thermoelectric Narrow Bandgap, Opto-electronics.

INTRODUCTION

The binary compounds of lead chalcogenides (PbS, PbTe, PbSe, etc.) have been known to form the basis of most devices for detectors/sensors such as photodetectors, infrared detectors (basically in medical diagnosis, night vision cameras, aircraft safety, manufacturing quality and control) and biological imaging devices. This can be ascribed to their peculiar behaviors which position them as suitable for these photo response applications. These materials are noted to exhibit large values of exciton Bohr radius, narrow direct band gap energies, and large dielectric constant which give rise to a strong quantum confinement effect for both electrons and holes in the materials, [1, 2]. In addition to photo sensing applications (infrared detectors, quantum dot lasers, etc.), most chalcogenides of the lead family of materials have found applications for thermoelectric devices (micro-coolers, micro-thermoelectric generators) as a result of its high figure of merit, good chemical stability, and low vapor pressure, [3]. The thermal conductivities at high temperatures have been known to be very low for simple structured materials and this unique feature has made them practical thermoelectric materials, [4]. Among the Pb-chalcogenide families, PbTe has been viewed as the most suitable material for the fabrication of optoelectronic photo-sensing devices because it works well in the infrared region. This can be attributed to the very narrow direct band gap energy in the order of 0.29 eV, large exciton Bohr radius of 150 nm as well as the high melting point of 900 K attributed to the material, [5]. Specifically, the PbTe material has found good applications in the infrared and thermoelectric devices fabrications used for

ISSN No. 2454-6194 | DOI: 10.51584/IJRIAS |Volume XI Issue II February 2026

infrared detectors, thermoelectric generators, environmental monitoring, and surveillance today as a result of their relatively high free carrier mobility, low Auger recombination rate and high thermoelectric figure of merit, [6]. The various parameters that determine the thermoelectric efficiency of PbTe for thermoelectric application have been x-rayed to be dependent on factors such as Debye temperature (K), Enthalpy, etc., [7]. Other factors considered imperative to the unusual behaviour of PbTe for device application have been greatly linked to the strong stoichiometric deviation of the order 1018 -1019cm^{-3} for electrically active intrinsic defects in the material, [8]. The positive temperature coefficient (dE_g/dT) and stability of the lattice for this material have been considered as yet another important factor that positions PbTe chalcogenide for its numerous applications, [9]. Doping of most lead chalcogenides in the case of PbTe with other materials has resulted in the alteration of most physical features including the structural and optical behaviour of the material for any desired application, [10]. To improve on the various unique properties of PbTe such as the high thermoelectric figure of merit ZT and others involves controlled manipulation of the structure and formation of lowdimensional systems of the material such as thin film structures based on existing properties, [11]. In this regard, the properties of most group IV-VI semiconductor materials have been reported to be improved for certain applications through the process of doping using different material elements, [12]. Crystallite size and lattice constant shrinkage as well as blue shift in bandgap have been observed for Sb-doped PbTe on both glass and FTO compared to the undoped sample as reported by [13]. The $Pb_{1-x}Ge_xTe$ thin films are high-index material in thin-film interference filters, as a result of their tunable optical properties as well as their superior mechanical properties, such as hardness and Young's modulus, [14]. NiTe-PbNiTe with an atomic ratio of 1.5:1 for electrode application has been found to deliver a high discharge capacity of 208.4 mAh g1 after 200 cycles hence, offering superior Li-ion storage over their single counterparts, [15]. The authors also showed that the electrochemical strength of the material is highly tunable by changing the Ni precursor ratios. The report of sintering of Ni to PbTe showed that various factors such as entropy, enthalpy, and Gibbs free energy of the reaction at room temperature and 793 K have been well repositioned for thermoelectric application according to [16]. The thermoelectric properties of PbTe thin films, deposited with different Ag concentrations using pulsed laser deposition (PLD) method have been reported by [17]. The authors inferred that the most thermoelectric properties of the films such as electrical resistivity as well as Seebeck coefficient were highly influenced as a result of Ag doping and the Ag-PbTe system was identified to lead to improved performance in the temperature range 510–540 K. They concluded that PLD can be extremely advantageous for the fabrication of a material of this nature for thermoelectric application.

In this report, the optical and structural properties of Ni-doped PbTe deposited via electrodeposition technique were investigated for their device applications.

MATERIALS AND METHOD

The materials used in the deposition of the Ni-doped PbTe thin films include the following; florine-doped tin oxide (FTO) conductive glass substrate, silver/silver chloride electrode, platinum rod, 100 ml glass beaker, distilled water, Potentiostat (model Zhaoxin: RXN-3010D), magnetic stirrer. Other materials include lead trioxonitrate (V), H_2SO_4, tellurium (IV) oxide, and nickel chloride hexahydrate. Three electrode configuration schemes of the electrodeposition technique were employed to deposit the thin films of Ni-PbTe at a constant potential of 4.0 volts. In the electrodeposition technique, the FTO conductive glass substrate was used as the working electrode, silver/silver chloride served as the reference electrode, and the platinum rod was used as the counter electrode. The 100 ml glass beaker served as the reaction container, distilled water was the reaction medium, Potentiostat (model Zhaoxin: RXN-3010D) was the DC supply unit and a magnetic stirrer was used to stir the solution mixture. To deposit the thin films of Ni:PbTe using the method on the FTO glass substrate, an aqueous electrolytic bath composed of 20 ml of 0.10 M lead trioxonitrate (V) mixed with 5 ml of 1.0 M H_2SO_4 (pH adjuster) was made and the mixture was stirred for 2 minutes. This was followed by the addition of 15 ml of 0.05 M tellurium (IV) oxide (TeO_2) and the solution was stirred for another 5 minutes. 4 ml of 0.010 M nickel chloride hexahydrate was finally added to the mixture and stirred for more 5 minutes. The three electrodes were immersed into the bath containing the electrolytic solution and 4 volts were maintained from the D.C supply unit and the setup was allowed for 1 minute. This process was repeated three times by optimizing the deposition time to study their effect on the properties of the films. Other parameters were allowed to be constant and the summary is displayed in Table 1.

ISSN No. 2454-6194 | DOI: 10.51584/IJRIAS |Volume XI Issue II February 2026

Table 1: Bath parameter for deposition time optimized Ni-PbTe thin films

0.1 M $Pb(NO_3)_2$	0.01 M $NiCl_2 \cdot 6H_2O$	0.05 M TeO_2	1.0 M H_2SO_4	Applied potential	Time
Vol. (ml)	Vol. (ml)	Vol. (ml)	Vol. (ml)	volts	(min.)
20.00	4.00	15.00	5.00	3.0	1.0
20.00	4.00	15.00	5.00	3.0	3.0
20.00	4.00	15.00	5.00	3.0	4.0
20.00	4.00	15.00	5.00	3.0	5.0

RESULTS AND DISCUSSION

Thin film thickness of the deposited Ni-doped PbTe thin films

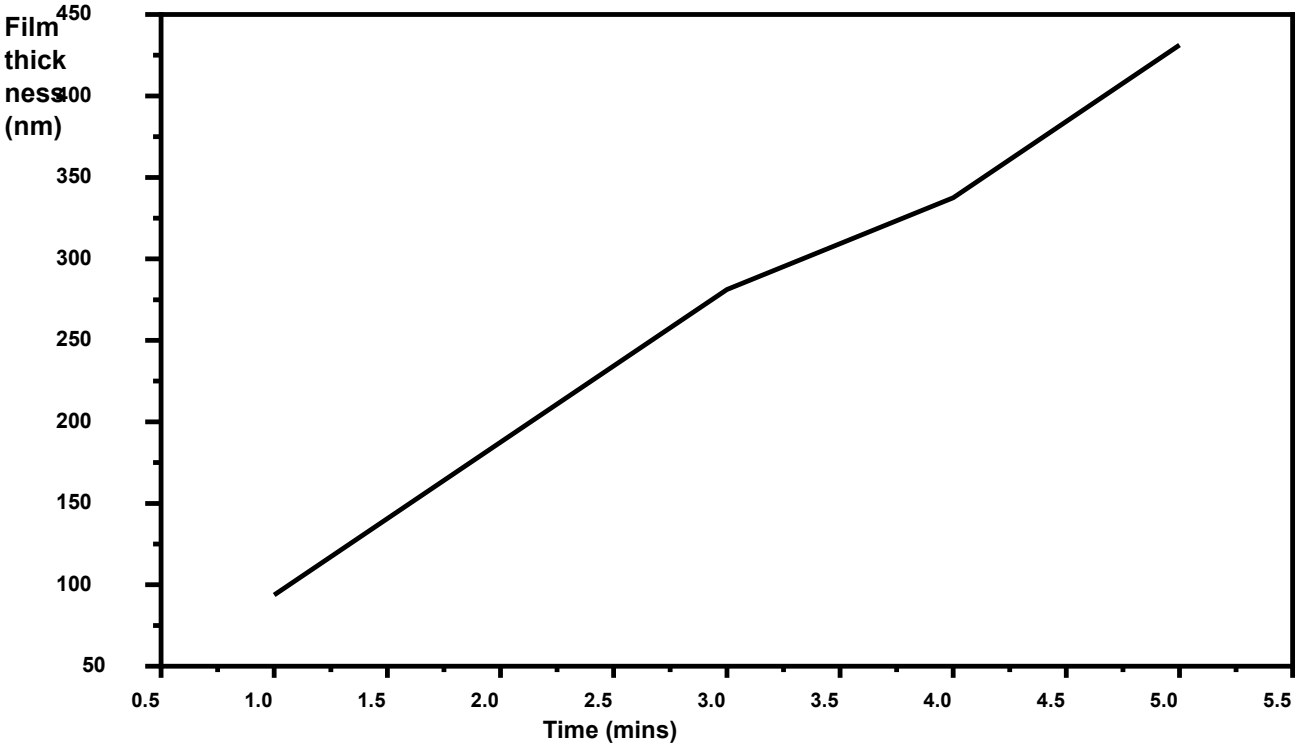

Figure 1: Graph of Film thickness against deposition time for the Ni: PbTe thin films

Figure 1 is the graph of film thickness against deposition time for the deposited thin films of Ni: PbTe to determine the variation of the thickness of the films with time. The thickness of each of the deposited thin films of Ni-doped PbTe was calculated using the gravimetric technique as provided by [18, 19].

$$t = \frac{\delta m}{\rho A} \qquad 1$$

Where,

δm represents the mass of the film, A is the surface area on which the films were deposited and ρ is the bulk density of the Ni: PbTe films. The mass of each of the samples was determined by taking the difference in mass between the mass of the glass substrate after the film deposition and its mass before the film deposition. The graph showed that the thickness of the films increased with an increase in deposition time. This result suggests that the thickness of the deposited thin films of Ni:PbTe can be controlled by the deposition period and as such various other properties of the films can be tailored for desired applications.

ISSN No. 2454-6194 | DOI: 10.51584/IJRIAS |Volume XI Issue II February 2026

Optical properties of the deposited Ni-doped PbTe thin films

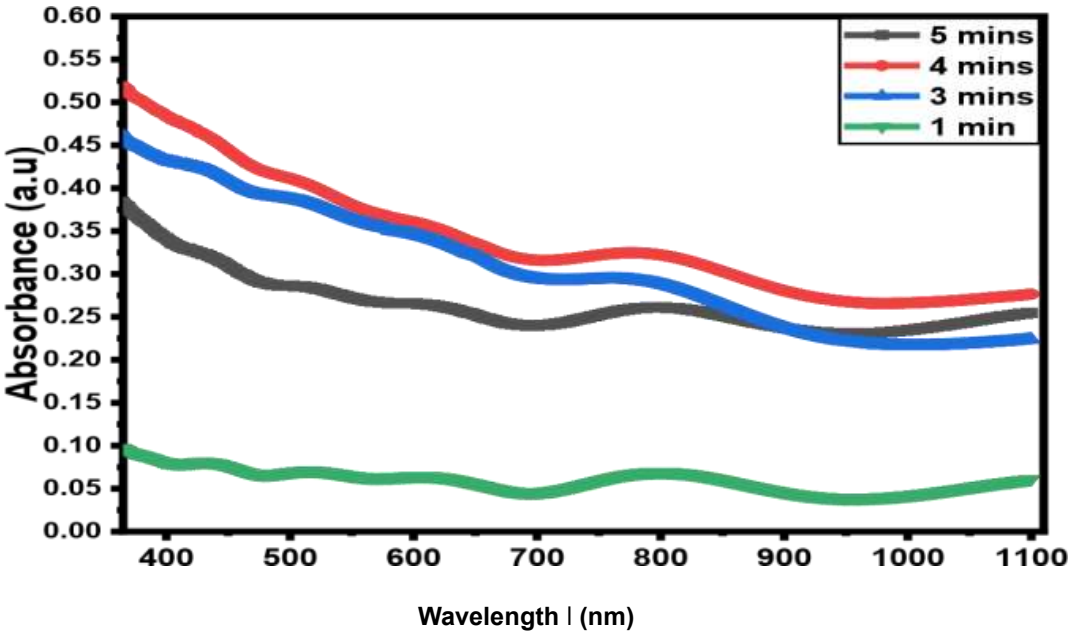

Figure 2: Graph of Absorbance against wavelength for the deposited Ni: PbTe thin films

Figure 2 is a graph of absorbance against wavelength for the deposited thin films Ni doped PbTe at different times of deposition to determine the influence of time variation on the absorbance property of the films. The graph showed that the films have low absorbance throughout the visible and near-infrared regions and equally decrease with an increase in wavelength. The absorbance of the films increased with an increase in deposition time up to the time of 4 mins (with absorbance in the range 0.27-052 in the VIS/NIR) and thereafter decreased to the value in the range 0.25-.037 at a deposition time of 5 mins. The film deposited at 1 min has the lowest absorbance of 0.10 in the VIS and NIR regions of the electromagnetic spectrum.

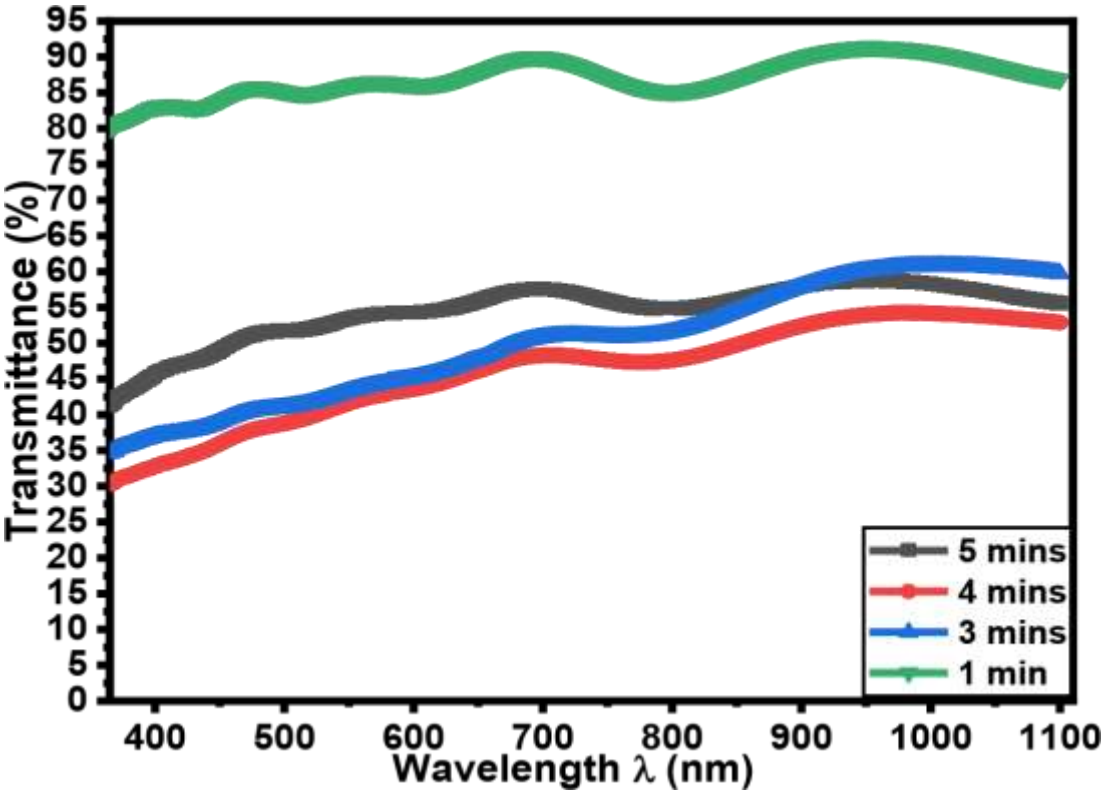

Figure 3: Graph of % Transmittance against wavelength for the deposited Ni: PbTe thin films

The graph of the percentage transmittance of the films against wavelength is presented in Figure 3. The transmittance was obtained using the relation as given by [20, 21].

ISSN No. 2454-6194 | DOI: 10.51584/IJRIAS |Volume XI Issue II February 2026

$$T = 10^{-A} \quad (2)$$

Where A is the measured absorbance of the films.

From the figure, it can be observed that the film deposited at a time of 1 min has the highest percentage transmittance of the order 80-90% throughout the VIS and NIR regions. The transmittance of the films however decreased as the time of deposition increased up to 4 mins and thereafter increased as time increased further to 5 mins. The transmittance of the films also increased with wavelength hence suggesting higher percentage values in the NIR region which position the films for cold window coating applications in the low temperate regions of the World.

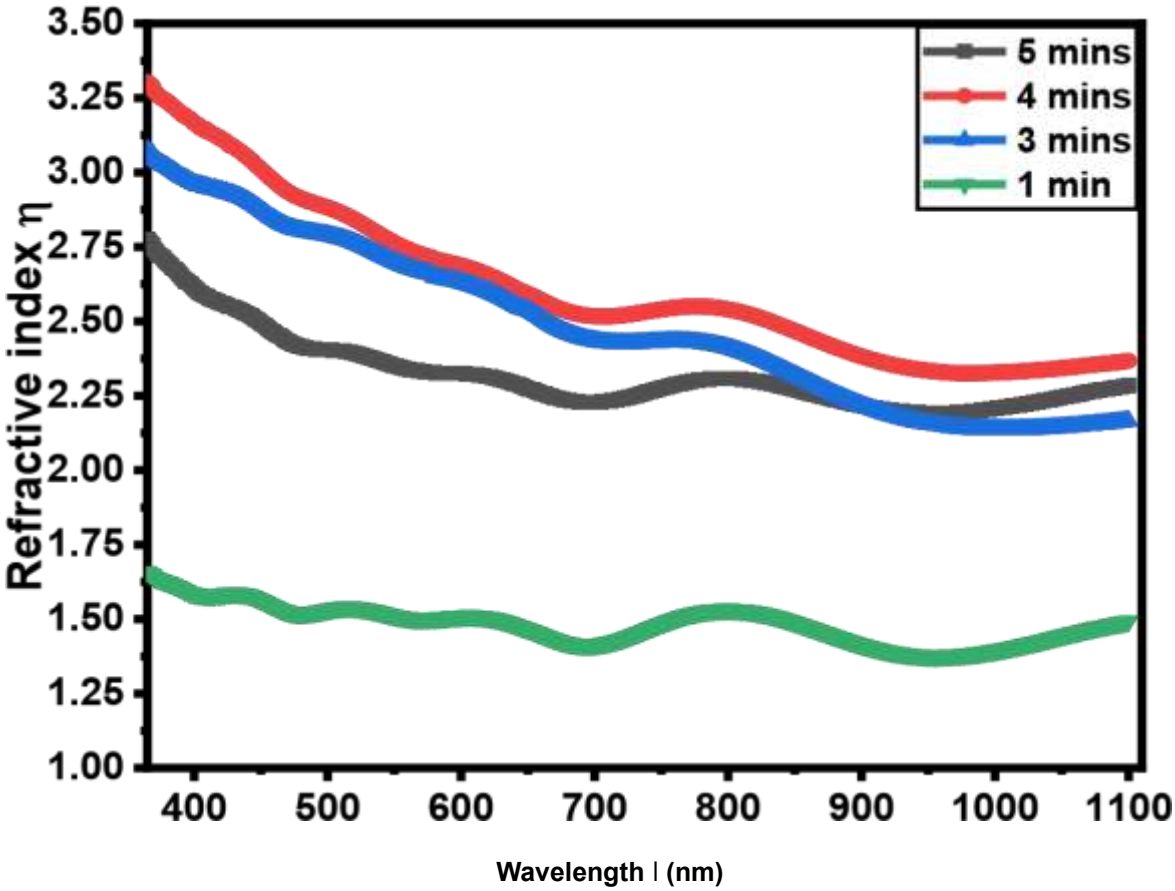

Figure 4: Graph of Refractive index against wavelength for the Ni: PbTe thin films

The graph of the refractive index against wavelength for the deposited thin films of Ni-doped PbTe at different deposition times to determine the effect of deposition time on the refractive index of the films is displayed in Figure 4. The refractive index was determined using the formula provided by [22].

$$n = \frac{1+\sqrt{R}}{1-\sqrt{R}} \quad (3)$$

Where R is the reflectance of the films.

The figure showed that the films have high refractive index values and initially increased with an increase in deposition time up to a time of 4 mins and thereafter started to decrease as time increased further to 5 mins. The film deposited at a time of 1 min has the lowest refractive index values in the range of 1.5 – 1.62 throughout the VIS and NIR regions while the film deposited at 4 mins has the highest values in the range of 2.5-3.25 in the VIS and NIR regions. The refractive index of the films also decreased with an increase in wavelength signifying lower values in the NIR region of the electromagnetic spectrum. The high refractive index values exhibited by the films are significant for many optoelectronic applications including optical fiber and waveguide devices.

ISSN No. 2454-6194 | DOI: 10.51584/IJRIAS |Volume XI Issue II February 2026

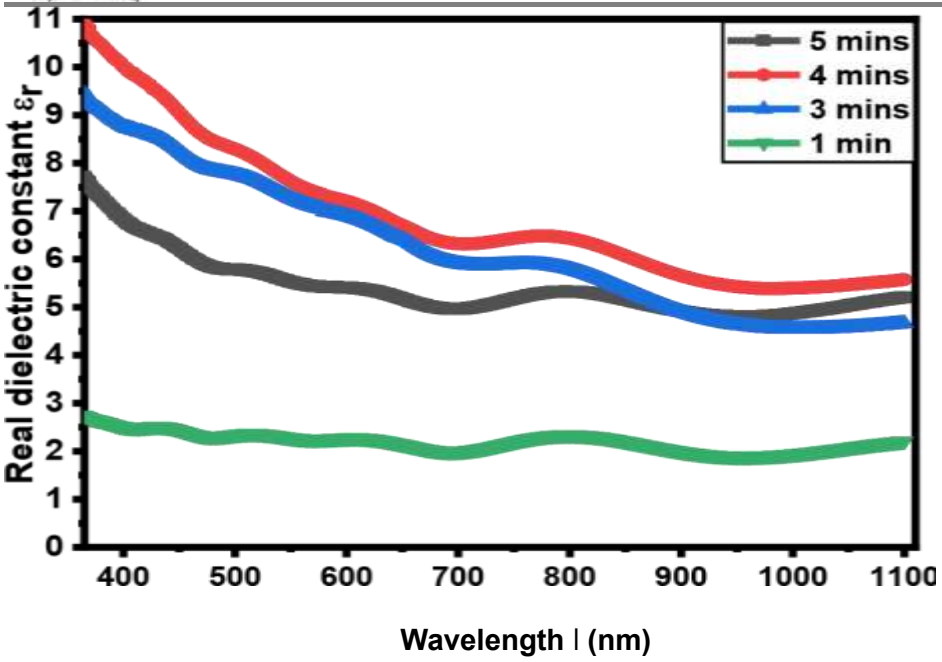

Figure 5: Graph of Real dielectric constant against wavelength for the Ni: PbTe thin films

The graph of the real dielectric constant of the films as a function of wavelength is shown in Figure 5. This property of the films was obtained using the relation given by [23].

$$\varepsilon_r = n^2 - k^2 \qquad 4$$

Where n and k are the refractive index and extinction coefficient of the deposited thin films.

From the figure it can be observed that the real part of the dielectric constant of the deposited thin films of Ni-doped PbTe increased as deposition time increased up to 4 mins and thereafter decreased as time of deposition increased further to 5 mins. The highest value of the real dielectric constant is exhibited by the film deposited at 4 mins with values in the range of 6-11 while the films formed at the time of 1 min have the lowest value of the order 2.5 throughout the VIS and NIR regions of electromagnetic spectrum. The real dielectric constant of the films also decreased with wavelength signifying lower values in the NIR regions.

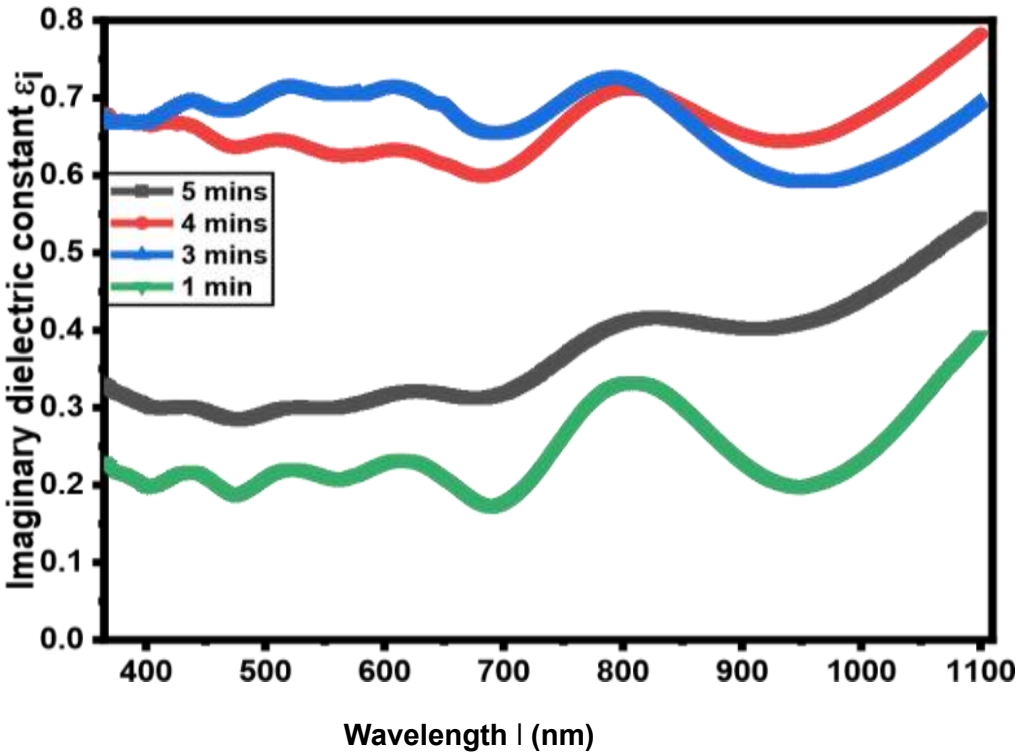

Figure 6: Graph of Imaginary dielectric constant against wavelength for the deposited Ni:PbTe thin films

ISSN No. 2454-6194 | DOI: 10.51584/IJRIAS |Volume XI Issue II February 2026

The plot of the imaginary part of the dielectric constant of the films as a function of wavelength to determine the effect of deposition time on the imaginary dielectric constant of the films is displayed in Figure 6. This other property of the films was calculated based on the relation provided by [24].

$$\varepsilon_i = 2nk \qquad 5$$

From the figure, the imaginary dielectric constant of the films is observed to increase as deposition time increased up to the time of 3 mins in the VIS while in the NIR region, it increased up to the time of 4 mins before decreasing to lower values as time increased to 5 mins. The film deposited at 3 mins has the highest values in the order of 0.66-0.75 in the VIS while the film formed at 4 mins has the highest value in the range of 0.66-0.8 in the NIR regions. On the other hand, the film deposited at a time of 1 min exhibits the lowest value in the range of 0.2-0.4 within the VIS and NIR regions. The imaginary dielectric constant of the films also tends to increase with wavelength which showed higher values in the NIR region than in the VIS.

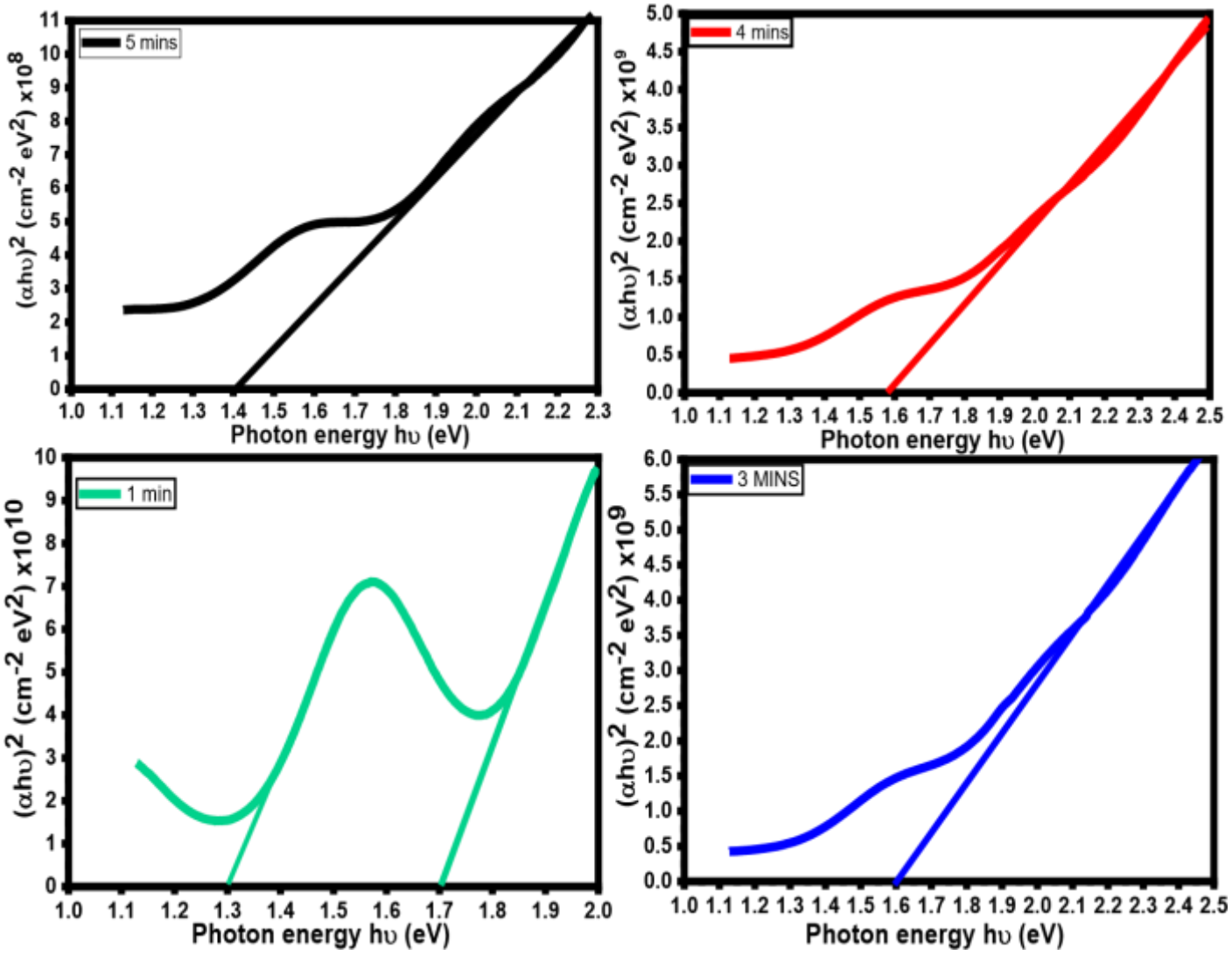

Figure 7: Plots of $(\alpha hv)^2$ as a function of Photon energy for the deposited Ni: PbTe thin films

Figure 7 shows the plots of $(\alpha hv)^2$ as a function of photon energy for the deposited thin films of Ni-doped PbTe to determine the direct bandgap energy of the films at different deposition times. The bandgap energy was calculated using the Tauc relation as provided by [25, 26].

$$(\alpha hv)^n = A(hv - E_g) \qquad 6$$

Where E_g is the bandgap energy of the films, hv is the photon energy, A is a constant and n is the transition factor which determines the nature of the transition. For direct allowed transition, n is 2 while for indirect transition it takes the value of half. From the figure, the bandgap energy values of the deposited thin film samples were estimated through extrapolation of the straight-line portions of the curves to the photon energy

ISSN No. 2454-6194 | DOI: 10.51584/IJRIAS |Volume XI Issue II February 2026

axes at which $(\alpha h\nu)^2$ equals zero. The figure revealed that the direct bandgap energy of the films tends to decrease as deposition time increases. The film deposited at a time of 1 min has bandgap energy in the range 1.3-1.7 eV, the film formed at 3 mins has a bandgap of 1.6 eV, 4 mins has a bandgap of 1.7 eV while the film deposited at 5 mins has a bandgap energy of 1.4 eV. These values of bandgap energies are strategic for many optoelectronic device applications such as photovoltaic cells and LED device fabrication.

Structural Properties of the deposited Ni: PbTe thin films

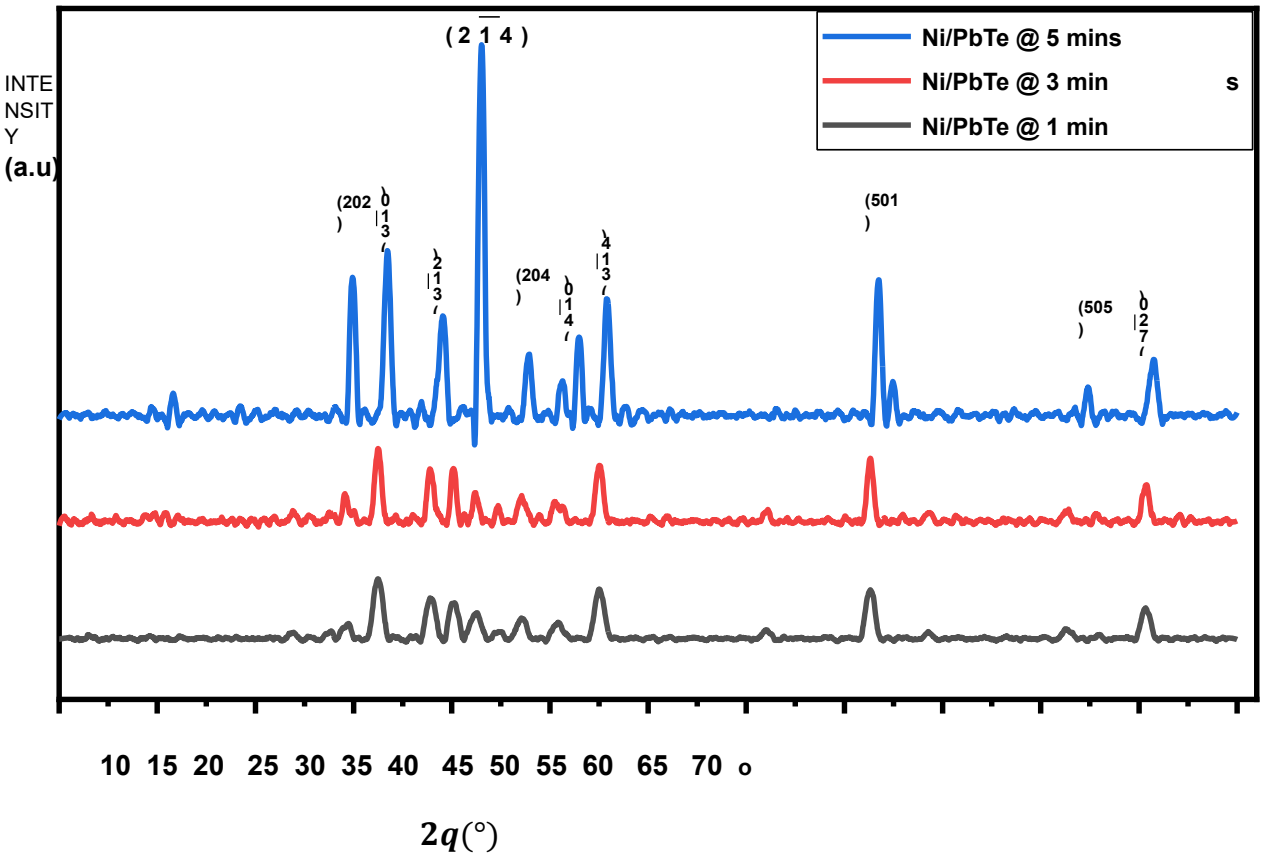

Figure 8. XRD patterns of the deposited PbTe:Ni thin films

Figure 8 is the XRD patterns of the deposited thin films of Ni-doped PbTe at deposition time variations of 1.0 min, 3.0 min, and 5.0 min to investigate their structural influence by time variation. The figure showed that the deposited thin films are crystalline as there exist sharp diffraction peaks in their XRD patterns. The sharp peaks in the XRD patterns of the films increased as deposition time increased with the intensity of the crystalline peaks being highest in the pattern of the film deposited at a time of 5 min. The diffraction peak positions of the deposited thin films match well with the standard JCPDS card NO; 00-200-2155, space group P 63 2 2 and crystal structure of hexagonal for lead nickel tellurium oxide ($Pb_3(Ni_{4.5}Te_{2.5}O_{15})$). The Williamson-Hall (W-H) analysis plots were carried out on the films for the diffraction peaks of the films deposited at a time of 1 min. 3 min. and 5 min. are displayed in Figure 9 to evaluate the crystal parameters of the films such as crystallite size, micro-strain, and dislocation density. The Williamson-Hall relation is as given by [27-29].

$$\beta_T Cos\theta = \frac{k\lambda}{D} + 4\varepsilon Sin\theta \qquad 7$$

Where β_T is the full weight at half maximum (FWHM) obtained by running Gaussian linear fits at the two theta peak positions, θ is the Bragg's angle (half two-theta position), k is the shape factor with constant value 0.9, λ is the wavelength of the X-ray Cu-α radiation used to probe the thin film materials, D represents the crystallite size of the films and ε is the micro-strain of the films. From the W-H relation, the scatter plot of $\beta_T Cos\theta$ on the vertical axis and $4Sin\theta$ on the horizontal axis gives a straight-line graph subject to linear fits of the plots, with $\frac{k\lambda}{D}$ representing the intercept on the vertical axis while the micro-strain ε becomes the slope of the plot.

ISSN No. 2454-6194 | DOI: 10.51584/IJRIAS |Volume XI Issue II February 2026

The dislocation density (δ) of the films was also estimated based on the Wilson equation as provided by [30]

$$\delta = \frac{1}{D^2}(lines/nm^2) \quad 8$$

Where D is the estimated crystallite size from the H-W plots.

The W-H analysis of the diffraction peaks subject to linear fittings according to the figure was used to calculate the crystallite size of the films as 15.018 nm, 21.337 nm, and 25.113 nm for the films deposited at 1 min., 3 min. and 5 min. respectively. Other crystal parameters like micro-strain and dislocation density were also estimated from the plots. In addition to W-H plot analysis, the average values of these crystal parameters were also calculated using the Scherrer relation and the obtained values were tabulated in detail in Table 2.

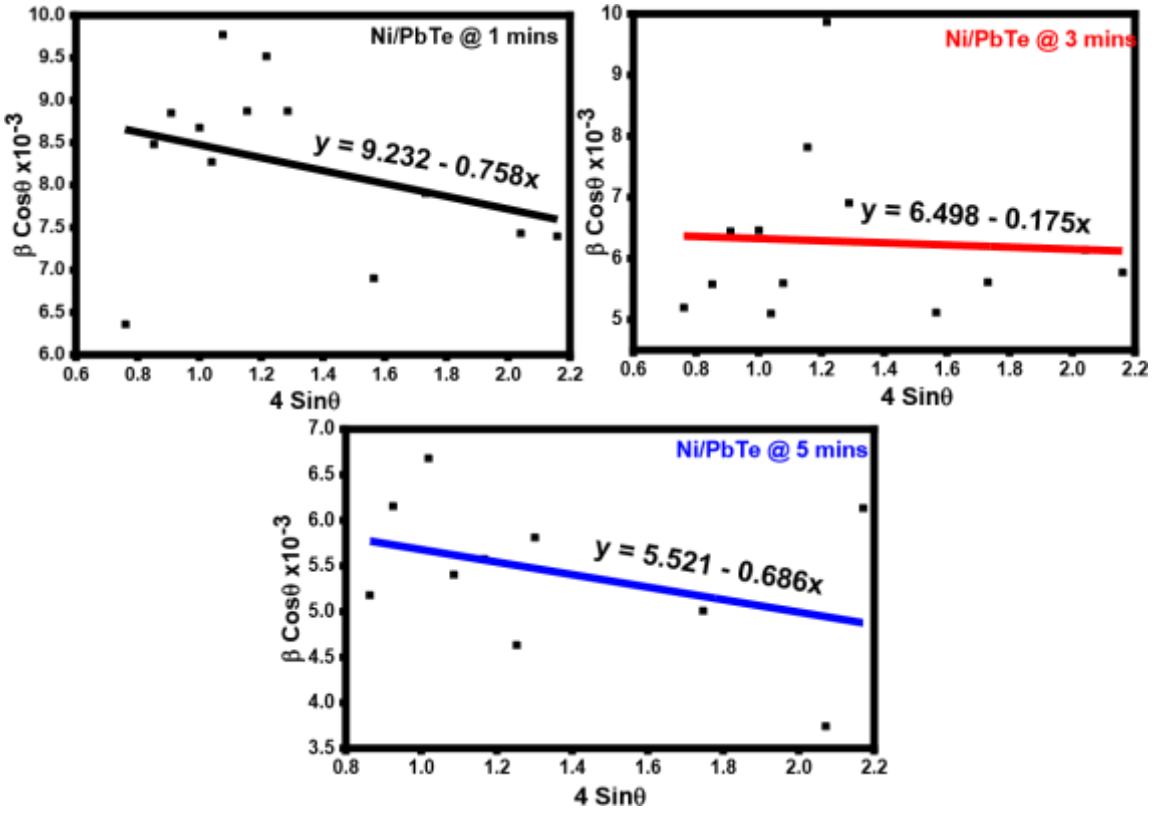

Figure 9: The Williamson-Hall (W-H) analysis of deposited Ni/PbTe thin films

Table 2: Crystal parameter estimations of the deposited Ni/PbTe thin films

Samples	Williamson-Hall (W-H) Analysis			Scherrer and Wilson relations calculations (average values)		
	Crystallite size (nm)	Micro-strain x10-3	Dislocation density x10^{-3} (nm^{-2})	Crystallite size (nm)	Micro-strain x10^{-3}	Dislocation density x10^{-3} (nm^{-2})
Ni/PbTe@1 min	15.018	0.758	4.433	17.049	7.094	3.591
Ni/PbTe@3 mins	21.337	0.175	2.196	22.059	5.342	2.132
Ni/PbTe@5 mins	25.113	0.686	1.586	26.170	4.464	1.569

Scherrer's and Wilson's relations for the calculation of crystallite size (D), micro-strain (ε), and dislocation density (**δ**) are given by [31, 32].

$$D = \frac{k\lambda}{\beta Cos\theta} \quad 10$$

$$\varepsilon = \frac{\beta}{4.Tan\theta} \quad 11$$

$$\delta = \frac{1}{D^2} \quad 12$$

Where β is the full weight at half maximum, k is the shape factor with a constant value of 0.9, and λ is the wavelength of the X-ray Cu-α radiation used to probe the thin film materials.

CONCLUSION

The Structural and optical characteristics of Ni-doped PbTe films fabricated using the electrochemical method have been investigated for device applications and the results showed that Ni doping has influences on the deposited film properties. These properties were investigated via UV-VIS spectroscopy and X-ray diffractometry techniques. The film's optical properties revealed that they have low absorbance behaviour but increased by an increase in deposition time. The films exhibit high values of transmittance but tend to decrease with an increase in the deposition period. The refractive index of the films ranges from 2.5-3.25 in the VIS and NIR regions for the samples deposited at higher deposition time and this value is significant for many optoelectronic applications including optical fibre and waveguide devices. The bandgap energy of the deposited Ni-doped PbTe is 1.3-1.7 eV for the film deposited at 1 min, 1.6 eV for 3 min, 1.7 for 4 mins eV, and 1.4 eV for 5 mins. These bandgap energy values are strategic for many optoelectronic device applications such as photovoltaic cells and LED device fabrication. The film thickness was discovered to increase as the deposition period increased and the result suggests that the deposited Ni:PbTe films can be controlled by the deposition period and as such various other properties of the films can be tailored for desired applications. The structural results showed that the deposited Ni-doped PbTe films exhibited crystalline structures which manifest most at higher deposition frequency. The crystal parameters of the films obtained using the W-H model and Scherrer relations are in close agreement with each other and the obtained values indicate strong crystallinity at a higher deposition period for the device application of the films.

ACKNOWLEDGEMENTS

The authors appreciate the team of scientists and technologists at Nano Research Laboratory, University of Nigeria Nsukka, Enugu State, Nigeria for their assistance in the analysis of their samples.

REFERENCES

1. Micone, J. A. H. (2018). Structural, electrical, and optical characterization of thiol-treated PbTe thin films infilled by alumina ALD (Doctoral dissertation, UC Irvine).
2. Nwori A. N., Ezenwaka L. N., Ottih I. E., Okereke N. A., Umeokwona N. S., Okoli N. L and Obimma I. O (2021). Effect of Deposition Voltage Variation on the Optical Properties of PbMnS Thin Films Deposited by Electrodeposition Method. Journal of Physics and Chemistry of Materials, 8(3), 1222.
3. [3] Zimin, S. P., Gorlachev, E. S., Naumov, V. V., Buchin, E. Y., & Zogg, H. (2011, April). Fabrication of porous nanostructured lead chalcogenide semiconductors for modern thermoelectric and optoelectronic applications. In Journal of Physics: Conference Series (Vol. 291, No. 1, p. 012023). IOP Publishing.
4. Takia, H., Rahman, M. A., Moshiur, R., Rahaman, M. M., & Hossen, K. (2022). The
5. Substantive Characteristics of Layered PbX (X= S, Se, and Te) Compounds: An ab-inito
6. Investigations. International Journal of Physics, 10(2), 102-110
7. Baghchesara, M. A., Yousefi, R., Cheraghizade, M., Jamali-Sheini, F., Saáedi, A., & Mahmmoudian, M. R. (2016). A simple method to fabricate an NIR detector by PbTe nanowires on a large scale. Materials Research Bulletin, 77, 131–137. doi:10.1016/j.materresbull.2016.0
8. Zhang, B., Cai, C., Hu, L., Wei, X., & Wu, H. (2011). Observation of regular defects formed on the surface of PbTe thin films grown by molecular beam epitaxy. Applied Surface Science, 257(6), 1986–1989. doi:10.1016/j.apsusc.2010.09.039

9. Zorah, M. (2024). A DFT Study the Electronic, Optical and Thermal Properties of XTe (X= Pb, Cd, Nb) for optoelectronic device Applications. Technium BioChemMed, 9, 28-40.
10. Akhmedov, T., Otajonov, S. M., Usmonov, Y., Khalilov, M. M., Yunusov, N., & Amonov, A. K. (2021, April). Optical properties of polycrystalline films of lead telluride with distributed stoichiometry. In Journal of Physics: Conference Series (Vol. 1889, No. 2, p. 022052). IOP Publishing.
11. Kungumadevi, L., & Sathyamoorthy, R. (2013). Synthesis of PbTe nanocubes, worm-like structures and nanoparticles by simple thermal evaporation method. Bulletin of Materials Science, 36(5), 771-778.
12. Ryabova, L., Chernichkin, V., Dobrovolsky, A., Kasiyan, V., Bel'Kov, V., Danilov, S., ... & Khokhlov, D. (2012, May). PbTe (In) films with variable microstructure for photodetection in IR and terahertz range. In Optical Sensing and Detection II (Vol. 8439, pp. 405-410). SPIE
13. Zimin, S. P., Gorlachev, E. S., Naumov, V. V., Buchin, E. Y., & Zogg, H. (2011, April). Fabrication of porous nanostructured lead chalcogenide semiconductors for modern thermoelectric and optoelectronic applications. In Journal of Physics: Conference Series (Vol. 291, No. 1, p. 012023). IOP Publishing.
14. Yost, A. J., Pimachev, A., Rimal, G., Tang, J., Dahnovsky, Y., & Chien, T. (2017). Effects of Mn dopant locations on the electronic bandgap of PbS quantum dots. Applied Physics Letters, 111(23), 1-5
15. Krataitong, C., Srichai, K., & Tubtimtae, A. (2021). Structural and optical properties of undoped and antimony-doped lead telluride thin films. Materials Letters, 285, 129085. (pp 1-14) doi:10.1016/j.matlet.2020.129085
16. Li, B., Xie, P., Zhang, S., & Liu, D. (2019). Infrared High-Index Coating Materials, PbTe and Pb1−xGexTe: Properties and Applications. IntechOpen. doi: 10.5772/intechopen.79272
17. Wang, Q., Zhu, J., Wang, H., Yu, S., & Wu, X. (2019). Anchoring NiTe domains with unusual composition on Pb0.95Ni0.05Te nanorod as superior lithium-ion battery anodes and oxygen evolution catalysts. Materials Today Energy, 11, 199–210. doi:10.1016/j.mtener.2018.12.001
18. Ferreres, X. R., Yamini, S. A., Nancarrow, M., & Zhang, C. (2016). One-step bonding of Ni electrode to n-type PbTe—A step towards fabrication of thermoelectric generators. Materials & Design, 107, 90-97.
19. Bellucci, A., Orlando, S., Medici, L., Lettino, A., Mezzi, A., Kaciulis, S., & Trucchi, D. M. (2023). Nanostructured Thermoelectric PbTe Thin Films with Ag Addition Deposited by Femtosecond Pulsed Laser Ablation. Energies, 16(7), 3216.
20. [18] Ravi, K., & Chitra, V. (2020). Structural and Surface morphology of Lead Selenide (PbSe) thin films. IOP Conference Series: Materials Science and Engineering, 932, 012133. doi:10.1088/1757899x/932/1/012133
21. Ezenwaka LN, Okoli NL, Okereke NA, Ezenwa IA, Nwori AN. Properties of Electrosynthesized Cobalt Doped Zinc Selenide Thin Films Deposited at Varying Time. Nanoarchitectonic. 2022; 3(1): 1-17. Available from: https://doi.org/10.37256/nat.3120221040
22. Nwori AN, Ezenwaka LN, Ottih IE, Okereke NA, Okoli NL. Study of the optical, structural and morphological properties of electrodeposited copper manganese sulfide (CuMnS) thin films for possible device applications. Trends in Sciences. 2022;19(17):5747
23. Kalu, U. A., Okpala U.V, Okereke N. A & Nwori A. N (2023). Structural and Optical Properties of Black Velvet Tamarind Doped Magnesium Sulfide Thin Films Grown by Sol-Gel Technique. Journal of Physics and Chemistry of Materials, 10(4), 01-09.
24. Ohwofosirai A, Femi M.D, Ngozika NA, Joseph T.O, Osuji R.U, Ezekoye B.A (2014). A study of the optical conductivity, extinction coefficient and dielectric function of CdO by successive ionic layer adsorption and reaction (SILAR) techniques. American Chemical Science Journal, 4(6):736-44.
25. Rajathi, S Kirubavathi K. and Selvaraju K (2017). Preparation of nanocrystalline Cd-doped PbS thin films and their structural and optical properties, Journal of Taibah University for Science, 11:6, 1296-1305, DOI: 10.1016/j.jtusci.2017.05.001.
26. Chauhan R, Srivastava AK, Mishra M, Srivastava KK. Effect of UV exposure on some optical properties of As-Se based chalcogenide glasses. Integrated Ferroelectrics. 2010;119(1):22-32.
27. Chanthong T, Intaratat W, Wichean TN (2023). Effect of Thickness on Electrical and Optical Properties of ZnO: Al Films, Trends in Sciences; 2093):6372-6372
28. Muomeliri, C. B., Ekpunobi, A. J., Okoli, D. N., Okafor, C., Mimi, J. D., Odikpo, O. E., ... & Okoli, N. L. (2024). Influence of Ti Doping on the Optical and Structural Properties of ZnTiO Thin
29. Films Deposited by Electrodeposition Technique. Journal of Materials Science Research and Reviews, 7(4), 493-506

30. Farag, A. A. M., Terra, F. S., Fahim, G. M. M., Ashery, A., Nasr, M., & El Okr, M. M. (2013). Structural and optical characterizations of nanocrystalline PbTe films prepared by flash evaporation and its device application. Optoelectronics and Advanced Materials-Rapid Communications, 7, 381-392.
31. Rajasekaran M, Arunachalam A, Kumaresan P (2020). Structural, morphological and optical characterization of Ti-doped ZnO nanorod thin film synthesized by spray pyrolysis technique. Materials Research Express,7(3), 036412.
32. Muomeliri C.B, Ekpunobi A.J, Okoli DN, Azubogu A. C, Nwori A.N, Diemiruyare M. J., Alex O. I., Okafor C. E, Ozobialu L, and Nwaodo A (2024). Effects of Deposition Periods on the Optical and Structural Properties of Electrochemically Deposited Nickel-Doped Zinc Oxide Thin Films. Journal of Physics and Chemistry of Materials, 11(3), 1-10.
33. Gareso PL, Heryanto H, Juarlin E, Taba P (2023). Effect of annealing on the structural and optical properties of ZnO/ITO and AZO/ITO thin films prepared by sol-gel spin coating. Trends in Sciences, 20(3), 6521
34. Ahmed, M. M., Tawfik, W. Z., Elfayoumi, M. A. K., Abdel-Hafiez, M., & El-Dek, S. I. (2019). Tailoring the optical and physical properties of La-doped ZnO nanostructured thin films. Journal of Alloys and Compounds, 791, 586-592.
35. Muomeliri, C. B., Okereke, N. A., Nwori, A. N., Okpala, U. V., & Okoli, N. L. (2024). Electrosynthesis and Characterizations of Aluminum Silver Selenide (Alagse2), Thin Films for Possible Device Applications. International Journal of Research and Scientific Innovation, 11(9), 954-961.